EurJIC
European Journal of Inorganic Chemistry

Full Papers
doi.org/10.1002/ejic.202100442

Chemistry Europe
European Chemical Societies Publishing

Green-Emissive Zn^{2+} Complex Supported by a Macrocyclic Schiff-Base/Calix[4]arene-Ligand: Crystallographic and Spectroscopic Characterization

Steve Ullmann,[a, b] Martin Börner,[a, c] Axel Kahnt,[c] Bernd Abel,[c, d] and Berthold Kersting*[a]

The macrocyclic calix[4]arene ligand H_2L comprises two non-fluorescent 2,6-bis-(iminomethyl)phenolate chromophores, which show a chelation-enhanced fluorescence enhancement upon Zn^{2+} ion complexation. Macrocyclic [ZnL] complexes aggregate in the absence of external coligands via intermolecular Zn–N bonds to give dimeric $[ZnL]_2$ structures comprising two five-coordinated Zn^{2+} ions. The absorption and emission wavelengths are bathochromically shifted upon going from the liquid ($\lambda_{max,abs}$ (CH_2Cl_2) = 404 nm, $\lambda_{max,em}$ (CH_2Cl_2) = 484 nm) to the solid state ($\lambda_{max,abs}$ = 424 nm (4 wt%, $BaSO_4$ pellet), $\lambda_{max,em}$ = 524 nm (neat solid)). Insights into the electronic nature of the UV-vis transitions were obtained with time-dependent density functional theory (TD-DFT) calculations for a truncated model complex.

Introduction

The synthesis of supramolecular assemblies[1] based on zinc complexes supported by Schiff-base ligands has been extensively investigated,[2] particularly for designing functional materials with specific sensoric,[3–10] catalytic[11–13] and photophysical properties.[14–26] Most studies have utilized four-coordinate zinc salen[27,28] and zinc salophen[29] complexes as building blocks,[30] which readily self-aggregate via intermolecular $Zn^{2+}\cdots$aryloxide bonds or form adducts with external Lewis basic groups.[31] The strong tendency of planar, four-coordinate zinc salen complexes to bind external N donor ligands in axial positions provides the basis for constructing supramolecular assemblies. Thus, helical complexes,[32,33] metallomacrocycles,[34–36] polynuclear clusters,[37,38] nanofibers[39,40] and other nanostructures[41,42] have all been constructed in this way.

The self-assembly properties of zinc complexes supported by other types of Schiff-base ligands is also attracting much interest.[43–46] Calix[4]arene-based salicylaldiminato ligands, for example, have turned out to be potent chelators for Zn^{2+} cations. Acyclic and cyclic ligands are readily synthesized by condensation reactions of appropriate calix[4]arene diamines and aromatic aldehydes. Rao has reported several N_2O_2 donor ligands built upon a 4-*tert*-butyl-calix[4]arene scaffold in the *cone* conformation.[47–51] Both monomeric and dimeric complexes with four-coordinated Zn^{2+} atoms are supported.[52–55] In the past few years, many fluorescent chemosensors for Zn^{2+} ions based on hybrid calixarene/Schiff-base ligands have been described.[56–65]

We have investigated previously the coordination chemistry of the macrocyclic ligand H_2L, comprising of 2,6-bis (iminomethyl)-4-*tert*-butylphenol and calix[4]arene head units (Figure 1).[66] This ligand enables the optical detection of Zn^{2+} ions among a series of biologically relevant metal cations in solution by a strong blue fluorescence emission. In the presence

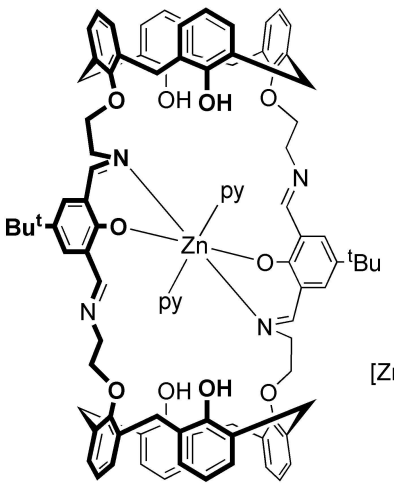

[ZnL(py)$_2$] (**1**)

Figure 1. Formula of the Zn^{2+} complex [ZnL(py)$_2$] (**1**) supported by the macrocyclic Schiff-base/calix[4]arene ligand H_2L (py = pyridine).

[a] *Dr. S. Ullmann, Dr. M. Börner, Prof. Dr. B. Kersting*
Institut für Anorganische Chemie, Universität Leipzig,
Johannisallee 29, 04103 Leipzig, Germany
E-mail: b.kersting@uni-leipzig.de
https://home.uni-leipzig.de/bkerst/
[b] *Dr. S. Ullmann*
Institut für Nichtklassische Chemie e.V.,
Permoserstraße. 15, 04318 Leipzig
[c] *Dr. M. Börner, Dr. A. Kahnt, Prof. Dr. B. Abel*
Leibniz Institute of Surface Engineering (IOM),
Department of Functional Surfaces,
Permoserstr. 15, 04318 Leipzig, Germany
[d] *Prof. Dr. B. Abel*
Wilhelm-Ostwald-Institut für Physikalische und Theoretische Chemie,
Universität Leipzig,
Linnéstraße 2, 04103 Leipzig, Germany

Supporting information for this article is available on the WWW under https://doi.org/10.1002/ejic.202100442

of Zn^{2+} ions the fluorescent intensity output of H_2L increased by a factor of ~10, presumably due to chelation of the Zn^{2+} ions reducing the PET quenching mechanism (PET = photo-induced electron transfer) of the imino functional groups. So far, only one Zn^{2+} complex supported by H_2L has been structurally characterized, namely mononuclear $[ZnL(py)_2]$ (py = pyridine) **1**. Herein, we report the crystal structure of the dimeric, base-free complex $[ZnL]_2$ (**2**), which shows a green fluorescence in the solid state. The optical properties of $[ZnL]_2$ have been investigated by diffuse reflectance, excitation, and emission spectroscopy, energy filtered photoelectron emission microscopy (PEEM), accompanying density functional theory (DFT) and time-dependent DFT (TD-DFT) calculations.

Results and Discussion

Synthesis and Characterization of $[ZnL]_2$ (2). The previously reported crystal structure of the $[ZnL(py)_2]$ complex **1** (py = pyridine) revealed a mononuclear complex with a six-coordinated Zn^{2+} atom, chelated by two imino N and two phenolato O atoms from $(L)^{2-}$ and two *cis*-oriented pyridine co-ligands (Figure 1).[66] The phenol groups of the two calix[4]arene units do not interact with the Zn^{2+} ion and remain protonated. There are also two dangling imine groups in this structure, the lone pairs of which pointing to the periphery of the complex. We reasoned that in the absence of pyridine, the [ZnL] monomers could be linked via these free imine-functions to form oligomeric or polymeric species as schematically illustrated in Scheme 1.

Acetonitrile was selected as crystallization medium since the coordination ability index (α^{TM}) is much lower than that of pyridine (MeCN: −0.2; py: +1.4).[67] A few crystals of $[ZnL]_2 \cdot 12MeCN$ (**2**·12MeCN) suitable for X-ray crystallography could be grown. Crystals of **2**·12MeCN are monoclinic space group $P2_1/n$. The crystal structure determination revealed the presence of a dimeric complex (Figure 2) and heavily disordered solvate molecules.

As can be seen two [ZnL] monomers are linked via two imine groups (Zn1-N4', Zn1'-N4). This aggregation mode is different from that seen for [Zn(salen)] complexes, which dimerize via phenolato bridges.[2,31,68] The neutral $[ZnL]_2$ complex has crystallographically imposed inversion symmetry. Molecules of $[ZnL]_2$ are well separated by the MeCN solvate molecules, which occupy the large interstitial voids in the structure. The closest intermolecular Zn···Zn distance at 16.7 Å is much longer than the intramolecular Zn···Zn distance at 6.7 Å.

Figure 3 shows a section of the structure of $[ZnL]_2$ with the calix[4]arene units omitted. Selected bond lengths and angles are summarized in Table 1. The Zn^{2+} ions are penta-coordinated and the coordination geometry is best described as distorted trigonal-bipyramidal, as suggested by the τ value of 0.63.[69] The two phenolate O atoms occupy the apical positions and the imine N donors form the base of the trigonal bipyramid. The distortions from the ideal coordination geometry are manifested in the N–Zn-N angles which deviate by as much as ~20° from the ideal 120° value. The Zn–O distances (mean value 2.014(3) Å) are shorter than the Zn–N distances (2.087(3) Å) and compare well with those reported for [Zn(salen)(py)][70,71] and other five-coordinated $Zn^{II}N_3O_2$ complexes.[72]

In terms of coordination mode, two kinds of bis(iminomethyl)phenolate units can be distinguished in this structure. One unit acts as a bidentate NO donor ligand towards one Zn^{2+} ion, and the remaining imine function is non-coordinating (N1). The other bis(iminomethyl)phenolate binds one Zn^{2+} in a bidentate and another Zn^{2+} ion in a monodentate fashion. The two types of bis(iminomethyl)phenol units are designated as bidentate (B) and tridentate (T) in Figure 3

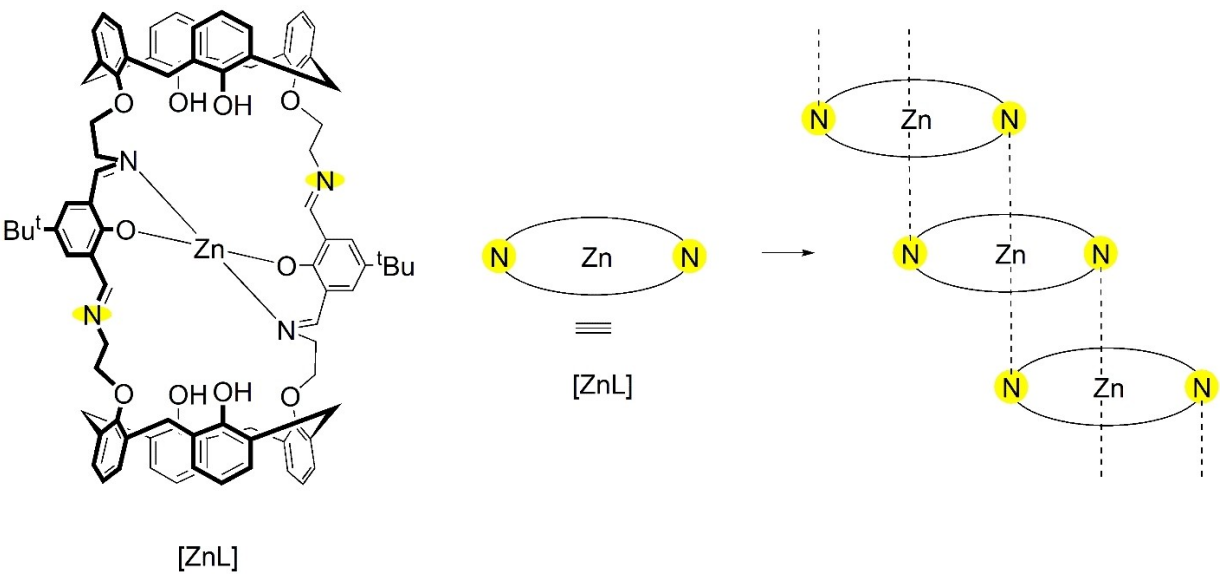

Scheme 1. Linking of [ZnL] monomers via the dangling imine-groups (highlighted) forming oligomeric or polymeric structures. The macrocyclic complex is represented by an ellipsoid for clarity.

Full Papers
doi.org/10.1002/ejic.202100442

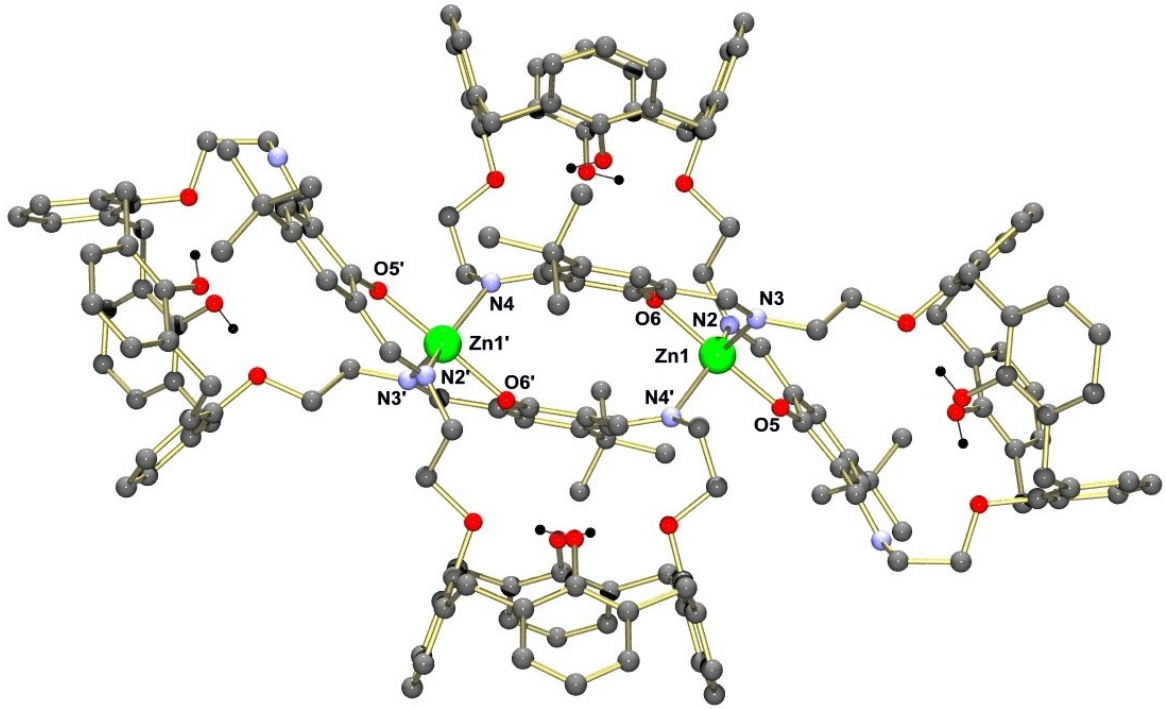

Figure 2. Molecular structure of the $[ZnL]_2$ complex **2** in crystals of **2**·12MeCN. Hydrogen atoms (except OH) are omitted for clarity. Symmetry code used to generate equivalent atoms 1-*x*, -*y*, -*z* (').

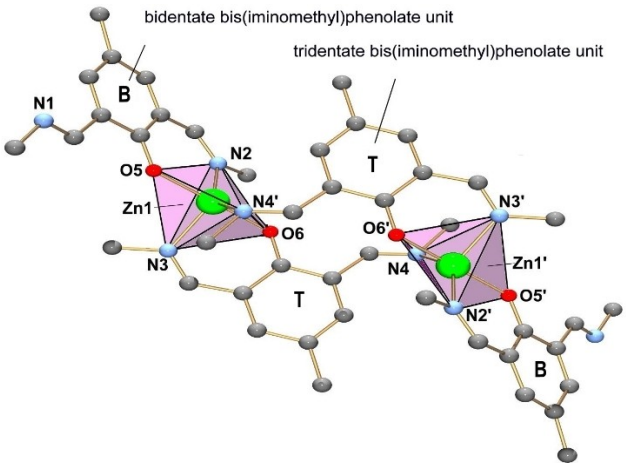

Figure 3. View of the central part of the structure of $[ZnL]_2$·12MeCN (calixarene units and *tert*-Bu groups omitted for clarity). B and T refer to the bidentate and tridentate bis(iminomethyl)-phenolate units, respectively. This complex fragment has been utilized for the DFT calculations.

and Figure 4. The planes through the imine groups in the bidentate entity are not coplanar with the aryl ring planes, as manifested by dihedral angles of 15.8° and 11.1° between the best planes through the imines (defined by the C^{ar}–C=N–C linkage) and the attached aryl ring. The corresponding angles in the tridentate unit are 11.1° and 30.3°.

Table 1. Experimental and calculated bond lengths / Å and angles /° for $[ZnL]_2$·12MeCN (**2**·12MeCN) and the truncated model complex $[Zn(L')_2]_2$ (for atom labels, see Figure 3, L' = 2,6-bis(N-methyl-iminomethyl)-4-methyl-phenolate).

	$[ZnL]_2$ (2)	$[Zn(L')_2]_{2,calc}$ [a]
Zn1-O5	2.002(3)	2.066
Zn1-O6	2.026(3)	2.096
Zn1-N2	2.066(3)	2.071
Zn1-N3	2.080(3)	2.118
Zn1-N4'	2.114(3)	2.160
C37-O5	1.297(5)	1.285
C53-O6	1.293(4)	1.286
O5-Zn1-O6	177.8(1)	177.1
O5-Zn1-N2	89.1(1)	88.8
O5-Zn1-N3	92.0(1)	92.5
O5-Zn1-N4'	91.2(1)	90.5
O6-Zn1-N2	89.2(1)	91.7
O6-Zn1-N3	87.5(1)	84.9
O6-Zn1-N4'	91.1(1)	91.2
N2-Zn1-N3	121.0(1)	127.3
N2-Zn1-N4'	140.4(1)	129.2
N3-Zn1-N4'	98.6(1)	103.5
δ(CN1=CC/ArO) [b]	15.8	0.4
δ(CN2=CC/ArO) [b]	11.5	0.7
δ(CN3=CC/ArO) [b]	11.1	16.0
δ(CN4=CC/ArO) [b]	30.3°	34.4

[a] B3LYP/def2-TZVP level of theory. The fragment shown in Fig. 3 (calix[4] arenes and *tert*-butyl groups replaced by methyl) has been utilized for the DFT calculations. [b] δ is the dihedral angle (C^{arO}-C^{ar}-C=N) that describes the tilting angle of the best planes through the imine and aryloxide groups.

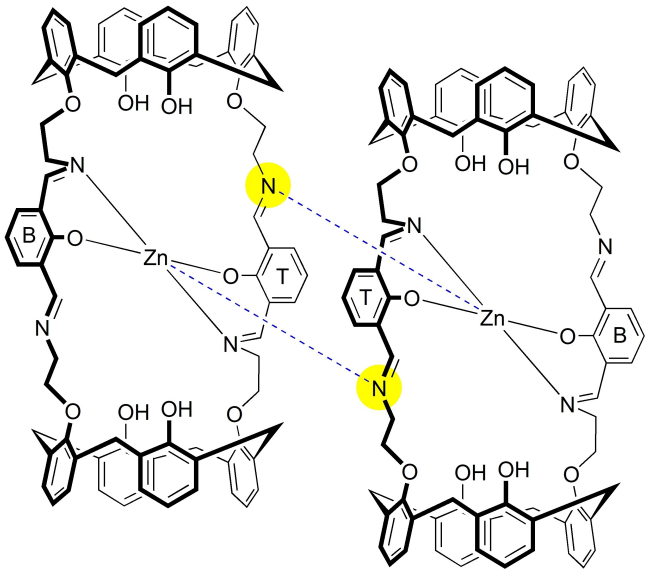

Figure 4. Mode of aggregation of two [ZnL] monomers in **2**, leading to bidentate (B) and tridentate (T) 2,6-bis(iminomethyl)phenolate moieties. The dashed lines refer to the intermolecular Zn–N bonding interactions.

Spectroscopic Properties

The spectroscopic properties of complex **2** were further studied by UV-vis diffuse reflectance, excitation, and emission spectroscopy as well as energy filtered photoelectron emission microscopy (PEEM). The UV-vis diffuse reflectance spectrum of the dimeric Zn^{2+} complex **2** (~4 wt% dispersed in $BaSO_4$ pellet) (Figure 5) is dominated by two intense absorption bands at 272 nm (not shown) and 424 nm. Intense bands at 286 nm are typical for calix[4]arenes, and have been assigned to $\pi\rightarrow\pi^*$ transitions.[73] The broad absorption maximum peaking at 424 nm in the blue region of the spectrum is attributed to strong $\pi\rightarrow\pi^*$ and weak ligand-to-ligand charge transfer (LLCT) excitations within the zinc-bound bis(iminomethyl)-4-*tert*-butylphenolate chromophores. Absorptions of similar energy have been observed for other Zn^{2+} complexes supported by bis(iminomethyl)-phenolate ligands in the liquid state.[74] TD-DFT calculations for the truncated model complex $[Zn(L')_2]_2$ (**2'**) also support the π-π^* and LLCT nature of the transitions (vide infra). The absorption maxima for **2** in CH_2Cl_2 solution (Figure S1) are observed at 272 and 403 nm.

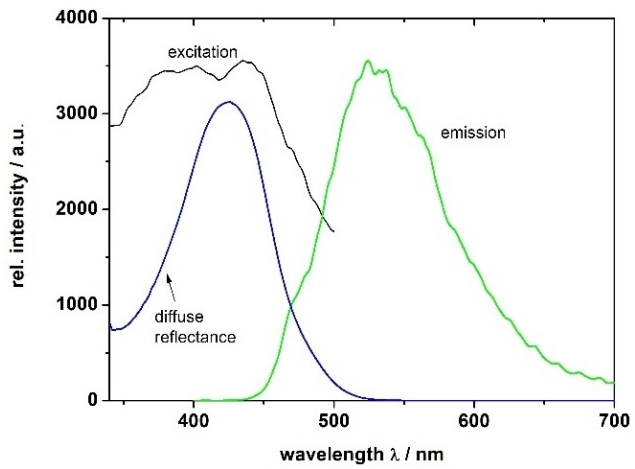

Figure 5. Kubelka-Munk converted diffuse reflectance UV-vis spectrum (blue curve, ~4 wt% finely dispersed in $BaSO_4$ powder), excitation spectrum (λ_{em} = 524 nm, black curve, neat powder), and emission spectrum (λ_{exc} = 435 nm, green curve, neat powder) of the solid Zn^{2+} complex **2** at 298 K.

It is well-known that Zn^{2+} binding can significantly enhance the rather weak, intraligand $^1(\pi$-$\pi^*)$ fluorescence emission of phenolate-based Schiff-base ligands owing to the inhibition of photo-induced electron transfer processes.[66] The zinc(II) complex **2** displays bright green emission under excitation with a blue LED lamp ($\lambda_{exc} = 395 \pm 5$ nm) in the solid state. The emission spectrum of **2** (neat powder, Figure 5) shows that the green fluorescence is related to an intense emission maximum at 524 nm. The corresponding excitation spectrum (monitored at 524 nm) shows a broad absorption band peaking at 435 nm, which is close to the absorption maximum at 424 nm seen in the UV-vis diffuse reflectance spectrum. The close resemblance of the steady state excitation and diffuse reflectance absorption spectra of **2** suggest that the emission arises from the lowest-energy S_1 state. Excitation and emission spectra were also recorded for complex **2** in halogenated solvents (CH_2Cl_2 (Figure S1), $CHCl_3$ (Figure S2)). To ascertain the integrity of complex **2** in these solvents, emission spectra were recorded in the concentration range from 10^{-4} to 10^{-7} mol·L^{-1} (Figure S3). The shape of the emission bands remains unchanged down to 10^{-6} mol·L^{-1} and the emission intensity decreases linearly with decreasing concentration, suggesting that **2** maintains its dimeric nature.[75] The absorption and emission maxima in solution appear slightly blue-shifted relative to those in the solid state. In our case, a red-shift by ~21 nm (from 403 nm in CH_2Cl_2 to 424 nm in solid state) is observed for the absorption maxima. Likewise, a red-shift of similar magnitude is observed for the emission maxima (494 nm ($CHCl_3$) vs 524 nm (solid state). This behavior is typical for π-π^* transitions of molecules with extended π-systems,[76] and can be rationalized in our case in terms of a larger delocalization of the π-system due to packing and/or intermolecular van der Waals interactions between the chromophores in the solid state. The fact that complex **1** emits at slightly higher energies ($\lambda_{max} = 484$ nm)[66] than complex **2** (494 nm) is not so clear cut. It may be due to a different degree of delocalization of the salicylaldimine π-systems caused by the differently coordinated Zn^{2+} ions in **1** (coordination number 6) and **2** (coordination number 5), respectively, although solvation effects cannot be ruled out (i.e. the emission spectrum of complex **1** was recorded in neat pyridine).

Energy filtered photoelectron emission microscopy (PEEM) measurements were conducted to approximate the energy of the S_0 state of complex **2** relative to vacuum. PEEM is conceptionally designed to obtain spatial resolved images of submicrometer structured systems. However, when measuring with an energy filter, binding energy resolved images are

obtainable.[77,78] PEEM on amorphous samples (which show no PEEM resolvable structures) can provide average binding energy of the emitted photo electrons. Under our experimental conditions – that is exciting with femtosecond pulsed (~50 fs pulse width) laser light at 357 nm (3.47 eV) – the photo electron emission takes place by a two-photon absorption process. The absorption of the first photon excites the sample into an excited state from which the absorption of the second photon, which occurs within the duration of the laser pulse, removes an electron from this excited state into the vacuum.[79,80] Our PEEM measurements performed for complex **2** (neat powder deposited on a Si/SiO_2 substrate) revealed a binding energy of −0.7 eV vs. vacuum (Figure S5), which is equivalent to a kinetic electron energy of 0.7 eV. Taking the binding energy of 0.7 eV and subtracting its absolute value from the energy of the two photons absorbed (2×3.4 eV) the energy level of the ground state of $[ZnL]_2$ below vacuum level is obtained, which amounts to −6.2 eV (please note, the negative value results from the convention that the vacuum level is assumed as 0 eV and energy levels below are marked with a negative sign).

DFT and TD-DFT calculations for $[Zn(L')_2]_2$ (2')

We performed density functional theory (DFT) and time-dependent DFT calculations on a truncated model complex $[Zn(L')_2]_2$ (**2'**), in order to analyze the spectroscopic properties of **2**. The ligand L' (=2,6-bis(N-methyl-iminomethyl)-4-methyl-phenolate) was used in place of H_2L for computational practicality. Initial coordinates for geometry calculations were derived from the crystal structure of **2**. The DFT-optimized geometry of **2'** (B3LYP/def2-TZVP level of theory) does not exactly reproduce the structural features of the experimentally determined structure for **2**, with some deviations seen in the immediate coordination environment of the Zn^{2+} ions. Thus, the average Zn–O bond lengths are ca. 0.06 Å longer and the Zn–N bonds are ca. 0.03 Å longer in the calculated structure of $[Zn(L')_2]_2$ (Table 1). Other main differences between the experimental and the calculated structures are (1) an increase in the τ parameter of ca. 0.17 (τ=0.80 $[Zn(L')_2]_2$, 0.63 $[ZnL]_2$), (2) a decrease of the N2-Zn1-N4' angles (140.4(1)° and 129.2°) in the experimental and calculated structures, respectively, and (3) a decrease in the dihedral angle between the best planes through the imine group (defined by C^{arO}-C^{ar}-C–N4) and the corresponding aryl ring of ca. 10° in the calculated relative to the experimental structure. These differences may be a consequence of the ligand simplifications of the Schiff-base unit and/or removal of the constraints imposed by the calix[4]arene units. The scaled calculated IR spectrum of $[Zn(L')_2]_2$ (B3LYP/def2-TZVP level of theory), on the other hand (Figure S7),[81] shows two strong imine ν(CN) stretches at 1617 cm^{-1} and 1595 cm^{-1} that are in excellent agreement with the experimental imine stretches for **2** at 1619 cm^{-1} and 1595 cm^{-1} (Figure S6), respectively. The good match between the calculated and experimental IR spectra suggests that the DFT calculations for $[Zn(L')_2]_2$ provide a reasonable description of the electronic structure for the bis(iminomethyl)phenolate moieties in **2**. Isosurface plots of the frontier orbitals of $[Zn(L')_2]_2$ are plotted in Figure S8. The highest-energy occupied molecular orbital (HOMO, #231, −5.31 eV) and the lowest-energy unoccupied molecular orbital (LUMO, #232, −1.67 eV) are in both cases derived from extended π-orbitals of the bis(iminomethyl) phenolate units. These findings are in line with previous DFT calculations for Zn^{2+} complexes supported by mixed Schiff-base/calix[4]arene ligands.[55] The TD-DFT computed absorption spectrum for the truncated model complex $[Zn(L')_2]_2$ is shown in Figure S9. Importantly, TD-DFT for the model complex properly reproduces the strong absorption seen in the blue edge of the spectra. The calculations suggest that the lowest allowed transitions result predominantly from strong $\pi\rightarrow\pi^*$ (calcd 378 nm, f=0.63) and weak interligand charge-transfer transition (calcd 416 nm, f=0.03). The nature of the latter transition can be regarded as a charge transfer from the π-system of the bidentate to the π-system of the tridentate bis(iminomethyl) phenolate ligand (Figure S10). The zinc ion does not contribute to these transitions.

Conclusion

The Zn^{2+} complex $[ZnL]_2$ supported by the macrocyclic Schiff-base/calix[4]arene-ligand H_2L exhibits a dimeric structure in the solid state. [ZnL] units are joined via two intermolecular Zn-N^{imine} bonds to afford two five-coordinated Zn^{2+} ions with distorted trigonal-bipyramidal coordination environments. The green fluorescence of complex **2** is related to an intense emission maximum at 524 nm, arising from the lowest-energy S_1 state of the $[ZnL]_2$ complex. This is attributed to the inhibition of photo-induced electron transfer processes in the Zn^{2+}-bound bis(iminomethyl)phenolate chromophores. It should be possible to construct other luminescent Zn^{2+} complexes by complexation of the calix[4]arene units.

Experimental Section

Materials and methods

All reagents and solvents were commercial grade and used without further purification. Diffuse reflectance spectra were collected on a Jasco V-670 UV-vis-NIR spectrophotometer equipped with a ARN-914 absolute reflectance measurement unit, a photomultiplier and a PbS photoconductive cell. Because of its strong absorbance, the sample of **2** was optically diluted with $BaSO_4$ (96 wt%), the baseline being recorded with a spectralon white standard. The diffuse reflectance (R) of the sample was converted to absorbance (T) via the Kubelka-Munk function: $T=(1-R)^2/(2R)$ implemented in the spectramanager software.[82] Solution absorption spectra were collected on a Jasco V-670 UV-vis-NIR spectrometer. Steady state fluorescence absorption and emission spectra were recorded on a PerkinElmer FL 6500 fluorescence spectrophotometer using precision cells for powder samples.

Compound $[ZnL]_2$ (2). To a suspension of H_2L,[66] (100 mg, 0.07 mmol) in EtOH (20 mL) was added $ZnCl_2$ (11 mg, 0.08 mmol). The suspension was stirred at reflux until the suspension became clear (2 h). The mixture was evaporated under reduced pressure to

give a bright yellow precipitate, which was filtered, washed with ethanol and Et_2O. The bright yellow powder was dried under vacuum to constant weight. Yield: 90 mg (86%). The analytical data for this material were identical with those given in the literature.[66] Crystals of $[ZnL]_2 \cdot 12MeCN$ (**2**·12MeCN) suitable for X-ray crystallography were obtained by slow evaporation of a solution of **2** in MeCN.

Crystal structure determination. The diffraction experiment was carried out on a STOE stadivari X-ray diffractometer at 180(2) K. The diffraction frames were processed with the STOE X-red software package.[83] The structures were solved by direct methods[84] and refined by full-matrix least-squares techniques on the basis of all data against F^2 using SHELXL-2018/3.[85] PLATON was used to search for higher symmetry.[86] All non-hydrogen atoms were refined anisotropically. H atoms were placed in calculated positions and allowed to ride on their respective C atoms, and treated isotropically using the 1.2-or 1.5-fold U_{iso} value of the parent C atoms. Unless otherwise noted, all non-hydrogen atoms were refined anisotropically. ORTEP-3 and POVray were used for the artwork of the structures.[87]

Crystal Data for $[ZnL]_2 \cdot x$MeCN ($x \sim 12$). $C_{200}H_{208}N_{20}O_{20}Zn_2$, $M_r =$ 3342.69 g/mol, monoclinic, space group $P2_1/n$, $a = 19.6291(6)$ Å, $b =$ 25.0766(7) Å, $c = 21.2339(7)$ Å, $\beta = 114.057(2)°$, $V = 9544.1(5)$ Å^3, $Z =$ 2 (the asymmetric unit contains one half of the formula unit), $\rho_{calcd} = 1.020$ g/cm^3, $T = 180(2)$ K, $\mu(CuK_\alpha) = 0.76$ mm^{-1} ($\lambda =$ 1.54186 Å), crystal size $0.07 \times 0.06 \times 0.05$ mm^3, 72865 reflections measured, 16156 unique, 5714 with $I > 2\sigma(I)$. Final $R_1 = 0.0569$ ($I > 2\sigma(I)$), $wR_2 = 0.1420$ ($I > 2\sigma(I)$), 1166 parameters, min./max. residual electron density $= -0.310/0.359$ e$^-$/Å^3. One calix[4]arene group was found to be disordered over two sites. The two orientations were modeled using the AFIX instruction implemented in SHELXL-2018/3 to give site occupancy factors of 0.53(2) and 0.47(2). Several MeCN solvent molecules in the structure of $[ZnL]_2 \cdot x$MeCN ($x \sim 12$) occupy interstitial spaces and were found to be highly disordered. It has not been possible to model this disorder, therefore, these were not included in the refinement (except for two MeCN molecules situated in the calix[4]arene cavities) and the e$^-$-density removed from the hkl file using the SQUEEZE routine implemented in PLATON.[88] The total potential solvent accessible void volume per unit cell was determined to be 2520 Å^3 and the electron count per unit cell is 440 e$^-$. This corresponds to ten acetonitrile molecules per formula unit. Due to the disordered solvate molecules the crystallinity of the crystals was not as good as desirable for a high-quality X-ray determination. At higher reflection angles, the intensity of reflections quickly deteriorated and, consequently, the ratio of observed / unique reflections is quite low, and the structure can only serve to confirm the atom connectivity.

PEEM measurements. PEEM measurements were performed in an IS-PEEM (FOCUS GmbH Hünstetten/Germany),[89] and a field of view of 270 μm was selected, from which the center (~100 μm in diameter) was selected for the determination of the binding energy. The sample was excited with a Fidelity-2 laser (Coherent). The fundamental wavelength (1070 nm) was frequency tripled to a central wavelength of 357 nm (3.4 eV) by an APE Harmonixx. The sample was illuminated via a normal incidence rhodium mirror in the Focus PEEM, and the laser power was set to 5.0 mW before entering the vacuum chamber through a window. The sample was prepared on a 1 cm^2 Si substrate (Plano GmbH), which was cleaned by ultrasonification in distilled water, acetone and isopropyl alcohol for 10 min each. $[ZnL]_2$ (**2**) was drop casted on Si/SiO_2 from a saturated toluene solution.

Density functional theory calculations. DFT calculations for the truncated $[Zn(L')_2]_2$ complex were performed with the ORCA program package (version 4.2.0).[90,91] Geometry optimizations were performed at the B3LYP / def2-TZVP level of theory[92–94] in a polarized continuum model (MeCN)[95] employing the resolution of identity and chain-of-spheres (RIJCOSX) approximation.[96,97] Geometry optimizations were performed using Ahlrichs' split-valence triple-z basis set def2-TZVP, which comprises polarization function for all atoms.[98,99] Calculations included the zeroth-order regular approximation (ZORA) for relativistic effects and a SARC/J auxiliary basis set.[100] Convergence criteria were set to tight for geometry optimizations and SCF calculations. The presence of energy minima/saddle points was checked by numerical frequency calculations. Since the vibration analysis were carried out under harmonic approximation, which usually overestimates vibrational frequencies, a scaling factor of 0.959 was applied for all calculated frequencies. Time-dependent DFT calculations were carried out at the same level of theory. Spectra were calculated using 30 vertical excitations and a line-width broadening of 1 eV.

Deposition Number 2084129 (for **2**) contains the supplementary crystallographic data for this paper. These data are provided free of charge by the joint Cambridge Crystallographic Data Centre and Fachinformationszentrum Karlsruhe Access Structures service www.ccdc.cam.ac.uk/structures.

Acknowledgements

We are grateful to Prof. Dr. H. Krautscheid for providing facilities for X-ray crystallographic measurements. This work was supported by the University of Leipzig and by the DFG (SPP2102, Light-controlled reactivity of metal complexes). Open Access funding enabled and organized by Projekt DEAL.

Conflict of Interest

The authors declare no conflict of interest.

Keywords: Calixarenes · Photophysical properties · Salicylaldiminato ligand · Self-assembly · Zinc

[1] a) J. W. Steed, D. R. Turner, K. J. Wallace, *Core Concepts in Supramolecular Chemistry and Nanochemistry*, Jon Wiley & Sons, New-York, **2007**; b) J.-M. Lehn, Supramolecular Chemistry; VCH, Weinheim, **1995**.
[2] C. J. Whiteoak, G. Salassa, A. W. Kleij, *Chem. Soc. Rev.* **2012**, *41*, 622–631.
[3] B. K. Kaletaş, R. M. Williams, B. König, L. De Cola, *Chem. Commun.* **2002**, 776–777.
[4] G. Consiglio, S. Failla, I. P. Oliveri, R. Purrello, S. Di Bella, *Dalton Trans.* **2009**, 10426–10428.
[5] E. C. Escudero-Adán, J. Benet-Buchholz, A. W. Kleij, *Inorg. Chem.* **2008**, *47*, 4256–4263.
[6] J. Tang, Y.-B. Cai, J. Jing, J.-L. Zhang, *Chem. Sci.* **2015**, *6*, 2389–2397.
[7] I. P. Oliveri, S. Failla, A. Colombo, C. Dragonetti, S. Righetto, S. Di Bella, *Dalton Trans.* **2014**, *43*, 2168–2175.
[8] P. Minei, E. Fanizza, A. M. Rodríguez, A. B. Muñoz-García, P. Cimino, M. Pavone, A. Pucci, *RSC Adv.* **2016**, *6*, 17474–17482.
[9] M. K. Paul, Y. D. Singh, N. B. Singh, U. Sarkar, *J. Mol. Struct.* **2015**, *1081*, 316–328.
[10] R. Brissos, D. Ramos, J. C. Lima, F. Yafteh Mihan, M. Borràs, J. de Lapuente, A. Dalla Cort, L. Rodríguez, *New J. Chem.* **2013**, *37*, 1046–1055.
[11] D. J. Darensbourg, P. Rainey, J. Yarbrough, *Inorg. Chem.* **2001**, *40*, 986–993.

[12] C. Mazet, E. N. Jacobsen, *Angew. Chem. Int. Ed.* **2008**, *47*, 1762–1765; *Angew. Chem.* **2008**, *120*, 1786–1789.
[13] A. Dalla Cort, P. De Bernardin, G. Forte, F. Y. Mihan, *Chem. Soc. Rev.* **2010**, *39*, 3863–3874.
[14] G. Yu, Y. Liu, Y. Song, X. Wu, D. Zhu, *Synth. Met.* **2001**, *117*, 211–214.
[15] S. Di Bella, I. Fragala, *New J. Chem.* **2002**, *26*, 285–290.
[16] A. C. W. Leung, J. H. Chong, B. O. Patrick, M. J. MacLachlan, *Macromolecules* **2003**, *36*, 5051–5054.
[17] P. Wang, Z. Hong, Z. Xie, S. Tong, O. Wong, C.-S. Lee, N. Wong, L. Hung, S. Lee, *Chem. Commun.* **2003**, 1664–1665.
[18] L. Rigamonti, F. Demartin, A. Forni, S. Righetto, A. Pasini, *Inorg. Chem.* **2006**, *45*, 10976–10989.
[19] G. Zhang, G. Yang, S. Wang, Q. Chen, J. S. Ma, *Chem. Eur. J.* **2007**, *13*, 3630–3635.
[20] O. Kotova, S. Semenov, S. Eliseeva, S. Troyanov, K. Lyssenko, N. Kuzmina, *Eur. J. Inorg. Chem.* **2009**, 3467–3474.
[21] Y. Hai, J.-J. Chen, P. Zhao, H. Lv, Y. Yu, P. Xu, J.-L. Zhang, *Chem. Commun.* **2011**, *47*, 2435–2437.
[22] F. Dumur, E. Contal, G. Wantz, D. Gigmes, *Eur. J. Inorg. Chem.* **2014**, 4186–4198.
[23] Q. Su, Q. L. Wu, G. H. Li, X. M. Liu, Y. Mu, *Polyhedron* **2007**, *26*, 5053–5060.
[24] M. Maiti, D. Sadhukhan, S. Thakurta, S. Roy, G. Pilet, R. J. Butcher, A. Nonat, L. J. Charbonnière, S. Mitra, *Inorg. Chem.* **2012**, *51*, 12176–12187.
[25] J. Cheng, X. Ma, Y. Zhang, J. Liu, X. Zhou, H. Xiang, *Inorg. Chem.* **2014**, *53*, 3210–3219.
[26] S. J. Malthus, S. A. Cameron, S. Brooker, *Inorg. Chem.* **2018**, *57*, 2480–2488.
[27] a) G. Consiglio, S. Failla, P. Finocchiaro, I. P. Oliveri, R. Purrello, S. Di Bella, *Inorg. Chem.* **2010**, *49*, 5134–5142; b) G. Consiglio, S. Failla, P. Finocchiaro, I. P. Oliveri, S. Di Bella, *Dalton Trans.* **2012**, *41*, 387–395.
[28] Q. Meng, P. Zhou, F. Song, Y. Wang, G. Liu, H. Li, *CrystEngComm* **2013**, *15*, 2786–2790.
[29] A. W. Kleij, *Dalton Trans.* **2009**, 4635–4639.
[30] a) M. Martínez Belmonte, S. J. Wezenberg, R. M. Haak, D. Anselmo, E. C. Escudero-Adán, J. Benet-Buchholz, A. W. Kleij, *Dalton Trans.* **2010**, *39*, 4541–4550; b) G. Salassa, M. J. J. Coenen, S. J. Wezenberg, B. L. M. Hendriksen, S. Speller, J. A. A. W. Elemans, A. W. Kleij, *J. Am. Chem. Soc.* **2012**, *134*, 7186–7192.
[31] G. Consiglio, S. Failla, P. Finocchiaro, I. P. Oliveri, S. Di Bella, *Inorg. Chem.* **2012**, *51*, 8409–8418.
[32] S. Mizukami, H. Houjou, Y. Nagawa, M. Kanesato, *Chem. Commun.* **2003**, 1148–1149.
[33] G. Zhang, Q. Li, G. Proni, *Inorg. Chem. Commun.* **2014**, *40*, 47–50.
[34] K. E. Splan, A. M. Massari, G. A. Morris, S.-S. Sun, E. Reina, S. T. Nguyen, J. T. Hupp, *Eur. J. Inorg. Chem.* **2003**, 2348–2351.
[35] C. T. L. Ma, M. J. MacLachlan, *Angew. Chem. Int. Ed.* **2005**, *44*, 4178–4182; *Angew. Chem.* **2005**, *117*, 4250–4254.
[36] A. W. Kleij, M. Kuil, D. M. Tooke, M. Lutz, A. L. Spek, J. N. H. Reek, *Chem. Eur. J.* **2005**, *11*, 4743–4750.
[37] S. J. Wezenberg, E. C. Escudero-Adán, J. Benet-Buchholz, A. W. Kleij, *Chem. Eur. J.* **2009**, *15*, 5695–5700.
[38] A. J. Gallant, J. H. Chong, M. J. MacLachlan, *Inorg. Chem.* **2006**, *45*, 5248–5250.
[39] a) J. K.-H. Hui, Z. Yu, M. J. MacLachlan, *Angew. Chem.* **2007**, *119*, 8126–8129; *Angew. Chem. Int. Ed.* **2007**, *46*, 7980–7983; b) J. K.-H. Hui, M. J. MacLachlan, *Dalton Trans.* **2010**, *39*, 7310–7319.
[40] I. P. Oliveri, S. Failla, G. Malandrino, S. Di Bella, *J. Phys. Chem. C* **2013**, *117*, 15335–15341.
[41] M. Piccinno, C. A. Angulo-Pachón, P. Ballester, B. Escuder, A. Dalla Cort, *RSC Adv.* **2016**, *6*, 57306–57309.
[42] I. P. Oliveri, G. Malandrino, S. Di Bella, *Dalton Trans.* **2014**, *43*, 10208–10214.
[43] G. Forte, I. P. Oliveri, G. Consiglio, S. Failla, S. Di Bella, *Dalton Trans.* **2017**, *46*, 4571–4581.
[44] A.-C. Chamayou, S. Lüdeke, V. Brecht, T. B. Freedman, L. A. Nafie, C. Janiak, *Inorg. Chem.* **2011**, *50*, 11363–11374.
[45] R. Pohl, V. A. Montes, J. Shinar, P. Anzenbacher Jr., *J. Org. Chem.* **2004**, *69*, 1723–1725.
[46] C. Evans, D. Luneau, *Dalton Trans.* **2002**, 83–86.
[47] R. K. Pathak, A. G. Dikundwar, T. N. Guru Row, C. P. Rao, *Chem. Commun.* **2010**, *46*, 4345–4347.
[48] R. K. Pathak, V. K. Hinge, M. Mondal, C. P. Rao, *J. Org. Chem.* **2011**, *76*, 10039–10049.
[49] R. Joseph, J. P. Chinta, C. P. Rao, *Inorg. Chem.* **2011**, *50*, 7050–7058.
[50] V. V. S. Mummidivarapu, V. K. Hinge, C. P. Rao, *Dalton Trans.* **2015**, *44*, 1130–1141.
[51] R. K. Pathak, V. K. Hinge, A. Rai, D. Panda, C. P. Rao, *Inorg. Chem.* **2012**, *51*, 4994–5005.
[52] M. Dey, J. P. Chinta, G. J. Long, C. P. Rao, *Indian J. Chem. Sect. A* **2009**, *48*, 1484–1491.
[53] R. Joseph, J. P. Chinta, C. P. Rao, *J. Org. Chem.* **2010**, *75*, 3387–3395.
[54] J. P. Chinta, B. Ramanujam, C. P. Rao, *Coord. Chem. Rev.* **2012**, *256*, 2762–2794.
[55] C. Laube, J. Taut, J. Kretzschmar, S. Zahn, W. Knolle, S. Ullmann, A. Kahnt, B. Kersting, B. Abel, *Inorg. Chem. Front.* **2020**, *7*, 4333–4346.
[56] C. D. Gutsche, *Calixarenes Revisited*, The Royal Society of Chemistry, Cambridge, 1998.
[57] B. Valeur, M. N. Berberan-Santos, *Molecular Fluorescence: Principles and Applications*, Wiley-VCH, Weinheim, 2012.
[58] Y. Fu, L. Mu, X. Zheng, J.-L. Zhao, C. Redshaw, X.-L. Ni, T. Yamato, *Dalton Trans.* **2013**, *42*, 3552–3560.
[59] H. M. Chawla, T. Gupta, *J. Lumin.* **2014**, 154, 89–94.
[60] S. De Solis, F. Elisei, T. Gunnlaugsson, *Supramol. Chem.* **2015**, *27*, 697–705.
[61] N. Kumar, P. X. Chi, Roopa, I. Leray, M.-H. Ha-Thi, *Calixarene-based Fluorescent Molecular Sensors*, in *Comprehensive Supramolecular Chemistry II*, Eds. J. L. Atwood, G. W. Gokel, L. J. Barbour, Volume 8, Elsevier, Amsterdam, 2017.
[62] R. Kumar, Y. Jung, J. S. Kim, *Fluorescent Calixarene Hosts*, in *Calixarenes and Beyond*, Eds. P. Neri, J. L. Sessler and M.-X. Wang, Chap. 28, 743−760, Springer, Switzerland, 2016.
[63] W. Sliwa, C. Kozlowski, *Calixarenes and Resorcinarenes, Synthesis, Properties and Applications*, Wiley-VCH, Weinheim, 2009.
[64] J. S. Kim, D. T. Quang, *Chem. Rev.* **2007**, *107*, 3780–3799.
[65] M. Song, Z. Sun, C. Han, D. Tian, H. Li, J. S. Kim, *Chem. Asian J.* **2014**, *9*, 2344–2357.
[66] S. Ullmann, R. Schnorr, M. Handke, C. Laube, B. Abel, J. Matysik, M. Findeisen, R. Rüger, T. Heine, B. Kersting, *Chem. Eur. J.* **2017**, *23*, 3824–3827.
[67] R. Díaz-Torres, S. Alvarez, *Dalton Trans.* **2011**, *40*, 10742–10750.
[68] M. Cano, L. Rodríguez, J. C. Lima, F. Pina, A. Dalla Cort, C. Pasquini, L. Schiaffino, *Inorg. Chem.* **2009**, *48*, 6229–6235.
[69] τ is defined as $(\alpha-\beta)/60°$, where α = largest angle, β = second largest angle ($\tau=1.0$ correspond to an ideal trigonal bipyramidal geometry; $\tau=0.0$ to an ideal square pyramidal geometry); A. W. Addison, T. N. Rao, J. Reedijk, J. Van Rijn, G. C. Verschoor, *J. Chem. Soc. Dalton Trans.* **1984**, 1349–1356.
[70] J. Reglinski, S. Morris, D. E. Stevenson, *Polyhedron* **2002**, *21*, 2175–2182.
[71] G. Salassa, J. W. Ryan, E. C. Escudero-Adán, A. W. Kleij, *Dalton Trans.* **2014**, *43*, 210–221.
[72] M. Kuil, I. Puijk, A. W. Kleij, D. M. Tooke, A. L. Spek, J. N. H. Reek, *Chem. Asian J.* **2009**, *4*, 50–57.
[73] L. J. Charbonnière, C. Balsiger, K. J. Schenk, J.-C. G. Bünzli, *J. Chem. Soc. Dalton Trans.* **1998**, 505–510.
[74] P. Roy, K. Dhara, M. Manassero, J. Ratha, P. Banerjee, *Inorg. Chem.* **2007**, *46*, 6405–6412.
[75] Below $c=10^{-6}$ mol·L^{-1}, a deviation from linearity can be observed indicative of the onset of deaggregation into monomeric [ZnL] species.
[76] M. Schwörer, H. C. Wolf, *Organische Molekulare Festkörper*, Wiley-VCH Verlag GmbH & Co. KGaA, Weinheim, 2005.
[77] M. Escher, N. Weber, M. Merkel, C. Ziethen, P. Bernhard, G. Schönhense, S. Schmidt, F. Forster, F. Reinert, B. Krömker, D. Funnemann, *J. Phys. Condens. Matter* **2005**, *17*, 1329–1338.
[78] O. Renault, R. Brochier, A. Roule, P.-H. Haumesser, B. Krömker, D. Funnemann, *Surf. Interface Anal.* **2006**, *38*, 375–377.
[79] S. Günther, B. Kaulich, L. Gregoratti, M. Kiskinova, *Prog. Surf. Sci.* **2002**, *70*, 187–260.
[80] O. Schmidt, M. Bauer, C. Wiemann, R. Porath, M Scharte, O. Andreyev, G. Schönhense, M. Aeschlimann, *Appl. Phys. B.* **2002**, *74*, 223–227.
[81] S. Kanchanakungwankul, J. L. Bao, J. Zheng, I. M. Alecu, B. J. Lynch, Y. Zhao, D. G. Truhlar, Database of Frequency Scale Factors for Electronic Model Chemistries – Version 4. https://comp.chem.umn.edu/freqscale/.
[82] G. Kortüm, *Reflexionsspektroskopie: Grundlagen, Methodik, Anwendungen*; Springer: Berlin, **1969**.
[83] *X-AREA and X-RED 32*; V1.35, STOE & Cie GmbH, Darmstadt, Germany, 2006.
[84] G. M. Sheldrick, *Acta Crystallogr.* **1990**, *A46*, 467–473.

[85] G. M. Sheldrick, *Acta Cryst.* **2015**, *C71*, 3–8.
[86] A. L. Spek, *PLATON – A Multipurpose Crystallographic Tool*; Utrecht University, Utrecht, The Netherlands, **2000**.
[87] L. J. Farrugia, *J. Appl. Crystallogr.* **1997**, *30*, 565.
[88] A. L. Spek, *Acta Crystallogr. Sect. D* **2009**, *65*, 148–155.
[89] A. Neff, F. Niefind, B. Abel, S. C. B. Mannsfeld, K. R. Siefermann, *Adv. Mater.* **2017**, *29*, 1701012.
[90] F. Neese, *Wiley Interdiscip. Rev.: Comput. Mol. Sci.* **2012**, *2*, 73–78.
[91] F. Neese, *Wiley Interdiscip. Rev.: Comput. Mol. Sci.* **2018**, 8:e1327.
[92] C. Lee, W. Yang, R. G. Parr, *Phys. Rev. B: Condens. Matter Mater. Phys.* **1988**, *37*, 785–789.
[93] B. Miehlich, A. Savin, H. Stoll, H. Preuss, *Chem. Phys. Lett.* **1989**, *157*, 200–206.
[94] A. D. Becke, *J. Chem. Phys.* **1993**, *98*, 5648.
[95] V. Barone, M. Cossi, *J. Phys. Chem. A* **1998**, *102*, 1995–2001.
[96] R. Izsak, F. Neese, *J. Chem. Phys.* **2011**, *135*, 144105.
[97] F. Neese, F. Wennmohs, A. Hansen, U. Becker, *Chem. Phys.* **2009**, *356*, 98–109.
[98] A. Schäfer, H. Horn, R. Ahlrichs, *J. Chem. Phys.* **1992**, *97*, 2571.
[99] A. Schäfer, H. Horn, R. Ahlrichs, *J. Chem. Phys.* **1994**, *100*, 5829–5834.
[100] D. A. Pantazis, X.-Y. Chen, C. R. Landis, F. Neese, *J. Chem. Theory Comput.* **2008**, *4*, 908–919.

Manuscript received: May 19, 2021
Revised manuscript received: July 30, 2021
Accepted manuscript online: August 4, 2021